Investigation into the ability of langbeinite-type K2M2(SO4)3 (M = Mn, Fe, Co and Ni) materials to accommodate Na

Driscoll, Laura; Driscoll, Lizzie; Slater, Peter

DOI:
10.1016/j.jssc.2020.121363

Document Version
Peer reviewed version

Citation for published version (Harvard):
Driscoll, L, Driscoll, L & Slater, P 2020, 'Investigation into the ability of langbeinite-type K2M2(SO4)3 (M = Mn, Fe, Co and Ni) materials to accommodate Na: the importance of the electronegativity of the framework cation', *Journal of Solid State Chemistry*, vol. 287, 121363. https://doi.org/10.1016/j.jssc.2020.121363

Investigation into the ability of langbeinite-type $K_2M_2(SO_4)_3$ (M = Mn, Fe, Co and Ni) materials to accommodate Na: the importance of the electronegativity of the framework cation

L.L. Driscoll[1*], E.H. Driscoll[1] and P.R.Slater[1*]

1. School of Chemistry, University of Birmingham, Edgbaston, Birmingham, B15 2TT, United Kingdom

Correspondence to:

Prof. P.R. Slater or Dr. Laura Driscoll

School of Chemistry, The University of Birmingham, Edgbaston, Birmingham, B15 2TT, United Kingdom

Abstract

In this work we report a study of the langbeinite-type $K_{2-x}Na_xM_2(SO_4)_3$ materials (M = Mn, Fe, Co and Ni) in order to evaluate the level of Na incorporation possible. The work showed that the level of Na incorporation decreased across the transition metal series, with the highest level of Na incorporation (up to x=1.3) observed for M=Mn. This trend does not appear to be related to the ionic radius of the transition metal, but rather its' electronegativity. We illustrate this relationship with the inclusion of our prior work on $K_{2-x}Na_xMg_2(SO_4)_3$ where even higher levels of Na were possible, and demonstrate that through co-doping with Mg, higher Na levels can be achieved for $K_{2-x}Na_xM_2(SO_4)_3$ materials (M = Mn, Fe). The dependence on the electronegativity of the divalent cation is attributed to greater electronegativity leading to enhanced polarization of the framework, thus allowing for greater stabilization of the smaller Na cation as it 'moves' towards the edge of the framework cage to better fulfil its' coordination requirements. Given the interest in related systems for Na ion battery applications, this work provides a new factor to consider when designing new materials for such applications.

Keywords: langbeinite, Na-ion, sulfate, sodium, oxyanion

Introduction

As global temperatures continue to rise due to over reliance on fossil fuels, renewable alternatives must play a role in order to tackle the growing threat of climate change. Rechargeable batteries will play a key role in such future infrastructure as they are able to store power produced by renewables (e.g. solar) during low demand and use when required during peak times. Although the predominant technology currently used is the Li-ion battery, cost and sustainability have driven research to explore alternative systems, such as Na, which may be better suited for large scale storage due to sodium's high natural abundance and hence lower cost.[1–3]

Three dimensional structures such as NaSICON and garnet have played an important role within the battery community due to a number of advantages such as favourable ionic conductivity and structural stability. NaSICON (Sodium (Na) Super Ionic Conductor) phases are a group of materials with the general formula $AyMM'(XO_4)_3$ ($0 \leq y \leq 4$) where A can either be an alkali, alkaline earth or rare earth cation (e.g. Li^+, Na^+, Mg^{2+} etc.), M/M' can be a number of multivalent transition metal cations (e.g. Mn^{2+}, Fe^{3+}, Ti^{4+}, Zr^{4+} and V^{5+}), and X is element that favours tetrahedral coordination (e.g. X=Si^{4+}, Ge^{4+}, P^{5+}, S^{6+}).[4–6] This chemical composition flexibility provides an opportunity to synthesise a wide range of compositions with varying A cation content. A notable example, $Na_3V_2(PO_4)_3$, can be used as an electrode (as either the cathode or anode) for Na-ion batteries with favourable electrochemical properties.[7–10] Structurally related Garnet materials, e.g. Al doped $La_3Zr_2Li_7O_{12}$ are also of great importance within the industry as potential solid state electrolytes for battery systems.[11]

A system which has been relatively unexplored for battery applications is the structurally similar potassium-based cubic langbeinite system, $K_2M_2(SO_4)_3$ (where M = Mg, Mn, Fe, Co or Ni). This system has a similar framework of corner linked octahedra and tetrahedra to that of the NaSICON structure. However, rather than four potential cavity sites for the alkali cation, there are only two sites, which are larger in size than those for the NaSICON structure. Hence the langbeinite structure is favoured for larger alkali cations such as K, Rb (Figure 1).[12]

[Fig 1 here]

Little literature exists with regards to the transition metal sulfate langbeinites, with most work focusing on the optical properties of the Mg system, $K_2Mg_2(SO_4)_3$, doped with rare earth metals[13–15]. In our previous work on this system, the Mg analogue was shown to be capable of up to 88% substitution of K for Na while still retaining the cubic langbeinite framework. [16] Furthermore, at high temperatures, even the Na end member ($Na_2Mg_2(SO_4)_3$) transformed to the cubic langbeinite structure, indicating that materials with the langbeinite structure may be of interest for Na-ion batteries.[17] In this respect, Tarascon *et al.* have recently shown the Fe and Cu analogues, $K_2(Fe/Cu)_2(SO_4)_3$, to be electrochemically active[18], however, with relatively poor performance compared to other potential Na-ion cathode systems containing sulfates. [19,20]

In this work, we present a synthesis and structural study to evaluate the ability of transition metal containing langbeinite systems, $K_2M_2(SO_4)_3$ (M = Mn, Fe, Co and Ni), to accommodate Na with a view to identifying whether they may be potential future targets as cathodes for Na-ion batteries, and to understand the limits placed on any Na incorporation. We also extend this work in investigate mixed systems containing Mn/Fe and Mg in order to evaluate the effect on the level of Na incorporation.

Experimental

All langbeinite samples were obtained through a wet chemical route; however, the synthetic route used varied depending on the metal cation selected to form the framework. Cations which were stable to oxidation in air were made through the following route. Stoichiometric amounts of potassium sulfate (Alfa Aesar, 99%), sodium sulfate (Sigma Aldrich, 99%) and $MSO_4{\cdot}xH_2O$ (where M = Mn, Co and Ni and x varies by metal from 1-7) were added to 20 cm^3 of water. The amounts were calculated based on producing 1 g of the desired phase (e.g. 1 g of $K_2Mn_2(SO_4)_3$ would require 0.3659g of K_2SO_4 and 0.7098 g of $MnSO_4{\cdot}H_2O$). The solutions were heated to ~60-70°C and stirred for approximately two hours. After mixing, the beakers containing the solutions were placed in an oven heated to 200°C for 2-3 hours. The precipitates were retrieved and ground and transferred to

an alumina crucible. The sample was then subjected to two heat treatments in air: 500°C/12hs/10°C min^{-1} followed by 650°C/12hs/10°C min^{-1} after regrinding. Samples containing Fe were made through a similar route, however, due to presence of impurities when using sodium sulfate as the sodium source, monosodium citrate and ammonium sulfate were used instead. Ascorbic acid (~20mg) was also added to prevent Fe oxidation in solution. The synthesis of these systems was more challenging, requiring modification to the synthesis conditions due to the sensitivity of Fe^{2+} to oxidation. Samples were initially dried at 100°C before undergoing a second heat treatment at 300-350°C/4-12hs/0.5°C min^{-1} under a nitrogen atmosphere in a tube furnace.

Sample purity and unit cell parameters were determined from powder X-ray diffraction using a Bruker D2 phaser (Co Kα radiation) or a Bruker D8 (Cu Kα radiation) operating in reflection mode. Rietveld refinements were carried out using the GSAS suite of programs. [21,22]

Results

$K_{2-x}Na_xMn^{(II)}_2(SO_4)_3$

In our previous study, $K_2Mg_2(SO_4)_3$ was capable of up to 88% substitution of K for Na while maintaining the cubic langbeinite structure at room temperature. [16] A similar doping strategy was applied to all transition metals that may be viable as cathodes for Na-ion batteries. The PXRD data and cell parameters for the manganese system are shown in **Figure 2 and Table 1**.

[Fig 2 here]

While significant Na could be accommodated in this system, it appears that the Na incorporation level is lower than for $K_2Mg_2(SO_4)_3$. The results show that the maximum sodium incorporation for the manganese system appears to be x = 1.3 (i.e. 65% substitution) as impurity phases were observed in compositions where x > 1.3. The most common impurity was attributed to $Na_2Mn_3(SO_4)_4$.[23] On Na doping, the structure was found not to vary significantly with increasing sodium concentration with the greatest changes observed between the compositions $K_2Mn_2(SO_4)_3$ and $K_{1.5}Na_{0.5}Mn_2(SO_4)_3$. The results of the refinements were similar to that observed in the $K_{2-x}Na_xMg_2(SO_4)_3$ system; for example,

one of the potassium/sodium sites shows a very slight displacement towards an edge of the cage and an overall decrease is observed in the S-O bond lengths when comparing the "K_2" and "$K_{2-x}Na_x$" compositions. The occupancies of the two sites were also refined and a slight preference was observed between the two sites. Potassium appears to favour the K2 site while sodium favours the K1 site, similar to prior studies of $K_{2-x}Na_xMg_2(SO_4)_3$. The metal oxygen bonds surrounding the K1 site (Mn1-O3) appear to decrease, suggesting the metal cage occupied by the alkali metal(s) is contracting as the smaller cation is doped onto the site. All other positions show a slight elongation (when x = 0.5), which may be suggestive of repulsion as the smaller cation moves to the edge of the cage to fulfil coordination requirements. When the Na content increases to x = 1.0, a contraction is observed in the Mn2-O2 bond, the metal-oxygen bonds surrounding the K2 site, which is consistent with sodium incorporation also into this site as the level of Na incorporation increases.

[Fig 3 here]

$K_{2-x}Na_xFe^{(II)}_2(SO_4)_3$

For the $K_{2-x}Na_xFe_2(SO_4)_3$ system, a further decrease in the ability to accommodate Na was observed. In this case, the highest sodium containing langbeinite phase that could be synthesised using this method was $KNaFe_2(SO_4)_3$ (i.e. 50% substitution). Due to the sensitivity of Fe^{2+} to oxidation, these systems proved to be the most difficult to prepare, leading to a modification of the synthesis conditions as noted in the experimental section. Even with these modified synthesis conditions, typically samples showed small impurities (**Figure 4**). Structure refinement (cell parameters are shown in Table 2) shows that sodium displays a similar small preference for the K2 site, however, the position of this site does not appear to shift to the same extent as observed in the magnesium and manganese langbeinite systems.

[Fig 4 here]

$K_{2-x}Na_xM^{(II)}_2(SO_4)_3$ (where M = Co & Ni)

The same doping strategy was attempted with the Co and Ni systems (Figure 4, Table 3). Based on size consideration alone, we would expect to see similar behaviour to that observed in the magnesium system, given the similar ionic radii for Co^{2+}, Ni^{2+} and Mg^{2+}. However, the maximum incorporation for the cobalt system appears to be much lower at x = 0.5, whereas the undoped nickel system, $K_2Ni_2(SO_4)_3$, could not be synthesized phase pure. This latter sample contains nickel sulfate and potassium sulfate impurities. Increasing the synthesis temperature beyond 650˚C was not practical due to the sample melting and reacting with the Al_2O_3 crucible, suggesting that an alternative synthetic method may be required in order to synthesize phase pure nickel phases. Sodium doping was still attempted, however, $Na_2M(SO_4)_2$ (M = Co, Ni) was observed to form, alongside the langbeinite phases, in both cobalt (for x>0.5) and nickel systems (all Na compositions), suggesting only a small level of sodium incorporation has been successful. This suggests that the accommodation of Na as $Na_2M(SO_4)_2$ is preferable to its incorporation in the langbeinite structure for Co (x>0.5) and Ni (all compositions).

[Fig 5 here]

Discussion

The results show that these transition metal containing langbeinite systems accommodate lower levels of Na than the Mg analogue previously reported [16]. Interestingly the level of Na content possible decreases as you move across the transition metal series, Mn-Fe-Co-Ni. This trend is not consistent with ionic radii considerations, since in such a case the Co, Ni systems would be expected to show the highest Na content, due to the similar ionic radii to Mg. Rather, it appears that the trend can be correlated with the electronegativity of the divalent cation. This is best shown in Figure 6, where the maximum sodium content has been plotted against the electronegativity of the divalent metal site within the framework. The greater the electronegativity of the divalent metal site, the lower the level of sodium incorporation. This suggests that as the framework increases in covalent

character, it is unable to stabilize the smaller sodium as it 'moves' to the edge of the cage to better fulfil its' coordination requirements (as observed most clearly in the Mg and Mn systems).[16]

[Fig 6 here]

For example, magnesium has a value of 1.3 on the Pauling scale while manganese is 1.6. Although a small difference, it suggests that the metal-oxygen bonding in the manganese system is more covalent than that of the magnesium system. This slight increase in covalency may reduce the polarization of the framework and therefore reduce the framework's ability to accommodate the smaller sodium ion. This agrees with the observed trend of decreasing sodium incorporation in langbeinite phases composed purely of transition metals with a greater electronegativity than manganese (e.g. Fe, Co and Ni). In order to provide further validation for this conclusion, mixed manganese/magnesium compositions $K_{2-x}Na_xMn_{2-y}Mg_y(SO_4)_3$, were attempted using a similar synthesis route. An initial test composition, $K_{0.5}Na_{1.5}Mn_{1.5}Mg_{0.5}(SO_4)_3$, was attempted to see if a low level of magnesium incorporation could help increase the sodium concentration in the material beyond the limits of the simple Mn system. After positive results; an attempt to increase the sodium concentration further was successfully demonstrated. Using the maximum sodium concentration found in the magnesium study, manganese was substituted with magnesium in $K_{0.25}Na_{1.75}Mn_{2-y}Mg_y(SO_4)_3$ for $0 \leq y \leq 1.0$. The diffraction patterns and cell parameter data for the resulting phases of this study are shown in Figure 7, Table 4.

[Fig 7 here]

The results show that the $Na_2Mn_3(SO_4)_4$ impurity decreases with increasing magnesium doping, such that a pure phase is obtained for y=1. The results of the study suggest that by co-doping with Mg, the sodium concentration can be increased to match that of the simple Mg based system.

Magnesium co-doping was also attempted for the Fe system. Given the potential application of this system as a Na ion battery material, only substitution of 25% of the Fe was investigated in order to

try to prepare a sample where in principle all the Na could theoretically be removed by relying on the Fe^{2+}/Fe^{3+} redox couple. A comparison of the resulting $K_{0.5}Na_{1.5}Fe_{1.5}Mg_{0.5}(SO_4)_3$ phase and $K_{0.5}Na_{1.5}Mn_{1.5}Mg_{0.5}(SO_4)_3$ are shown in Figure 8. The resulting PXRD patterns show successful synthesis of the Fe langbeinite phase with no obvious impurities, illustrating again the beneficial effect of Mg in increasing the achievable Na content. The same strategy was applied to both Co and Ni systems; however, doping was unsuccessful, possibly attributed to the higher stability of the $Na_2M(SO_4)_2$ phase compared to the langbeinite for these systems. Figure 6 has been updated to reflect the new Mg doped compositions which add further support for the correlation of the Na content with the electronegativity of the divalent cation (Figure 9).

[Figure 9 here]

Conclusions

In this work, we have assessed the ability of langbeinite-type materials containing first row transition metals to accommodate Na in place of K. The results show that frameworks composed of either Mn or Fe are better able to accommodate sodium compared to Co and Ni. In conjunction with our prior results for Mg based systems, this is attributed to the greater electronegativity of these transition metals, which leads to enhanced polarization of the framework thus allowing for greater stabilization of the smaller alkali cation as it 'moves' towards the edge of the framework cage to better fulfil its' coordination requirements. Therefore, the results suggest that, in order to improve the framework's ability to incorporate a greater proportion of sodium, doping strategies should focus on modifying the framework to be more ionic in character. Based on this initial assessment, co-doping on the transition metal site with Mg was attempted. The results showed that co-doping $K_{2-x}Na_xM_2(SO_4)_3$ (M= Mn, Fe) systems with Mg led to an increase in the amount of Na that could be incorporated into the structure, adding further weight to the above conclusions with regard to the importance of the electronegativity of the divalent cation. Overall, this study suggests that

electronegativity can be an important factor to consider when determining doping strategies for framework-type materials.

Acknowledgements

We would like to thank the University of Birmingham/Midlands Energy Consortium for funding (studentship to LD).

References

[1] M.D. Slater, D. Kim, E. Lee, C.S. Johnson, Sodium-ion batteries, Adv. Funct. Mater. 23 (2013) 947–958. doi:10.1002/adfm.201200691.

[2] A. Pehlken, S. Albach, T. Vogt, Is there a resource constraint related to lithium ion batteries in cars?, Int. J. Life Cycle Assess. 22 (2017) 40–53. doi:10.1007/s11367-015-0925-4.

[3] E.H. Driscoll, L.L. Driscoll, P.R. Slater, Na-Ion Batteries: Positive Electrode Materials , Encycl. Inorg. Bioinorg. Chem. (2019) 1–14. doi:10.1002/9781119951438.eibc2686.

[4] N. Anantharamulu, K. Koteswara Rao, G. Rambabu, B. Vijaya Kumar, V. Radha, M. Vithal, A wide-ranging review on Nasicon type materials, J. Mater. Sci. 46 (2011) 2821–2837. doi:10.1007/s10853-011-5302-5.

[5] F. Chen, V.M. Kovrugin, R. David, O. Mentré, F. Fauth, J.-N. Chotard, C. Masquelier, A NASICON-Type Positive Electrode for Na Batteries with High Energy Density: $Na_4MnV(PO_4)_3$, Small Methods. 3 (2019) 1800218. doi:10.1002/smtd.201800218.

[6] J.B. Goodenough, H.Y.-P. Hong, J.A. Kafalas, Fast Na^+-ion transport in skeleton structures, I (1976) 203–220. doi:10.1016/0025-5408(76)90077-5.

[7] Z. Jian, L. Zhao, H. Pan, Y.S. Hu, H. Li, W. Chen, L. Chen, Carbon coated $Na_3V_2(PO_4)_3$ as novel electrode material for sodium ion batteries, Electrochem. Commun. 14 (2012) 86–89. doi:10.1016/j.elecom.2011.11.009.

[8] Y. Lyu, Y. Liu, Z.E. Yu, N. Su, Y. Liu, W. Li, Q. Li, B. Guo, B. Liu, Recent advances in high energy-density cathode materials for sodium-ion batteries, Sustain. Mater. Technol. 21 (2019) 1–21. doi:10.1016/j.susmat.2019.e00098.

[9] X. Li, S. Wang, X. Tang, R. Zang, P. Li, P. Li, Z. Man, C. Li, S. Liu, Y. Wu, G. Wang, Porous $Na_3V_2(PO_4)_3$ /C nanoplates for high-performance sodium storage, J. Colloid Interface Sci. 539

(2019) 168–174. doi:10.1016/j.jcis.2018.12.071.

[10] X. Zhang, X. Rui, D. Chen, H. Tan, D. Yang, S. Huang, Y. Yu, $Na_3V_2(PO_4)_3$: An advanced cathode for sodium-ion batteries, Nanoscale. 11 (2019) 2556–2576. doi:10.1039/c8nr09391a.

[11] V. Thangadurai, S. Narayanan, D. Pinzaru, Garnet-type solid-state fast Li ion conductors for Li batteries: critical review., Chem. Soc. Rev. 43 (2014) 4714–27. doi:10.1039/c4cs00020j.

[12] K.K. Rangan, J. Gopalakrishnan, New Titanium-Vanadium Phosphates of Nasicon and Langbeinite Structures, and Differences between the Two Structures toward Deintercalation of Alkali Metal, J. Solid State Chem. 109 (1994) 116–121. doi:10.1006/JSSC.1994.1080.

[13] A. Souamti, M. Kahlaoui, B. Mohammed, A. Diego Lozano-Gorrín, D.B.H. Chehimi, Synthesis, structural and electrochemical properties of new ytterbium-doped langbeinite ceramics, Ceram. Int. 43 (2017) 10939–10947. doi:10.1016/j.ceramint.2017.05.132.

[14] A. Souamti, I.R. Martín, L. Zayani, M.A. Hernández-Rodríguez, K. Soler-Carracedo, A.D. Lozano-Gorrín, E. Lalla, D. Ben Hassen Chehimi, Synthesis, structural characterization and optical study of Dy^{3+}-doped langbeinite salts, J. Lumin. 177 (2016) 160–165. doi:10.1016/j.jlumin.2016.04.045.

[15] H. Marzougui, D. Ben Hassen-Chehimi, Study of structural and optical properties of Nd^{3+} doped $K_2Mg_2(SO_4)_3$ langbeinite salts, Inorg. Chem. Commun. 104 (2019) 201–206. doi:10.1016/j.inoche.2019.04.009.

[16] I.A. Trussov, L.L. Driscoll, L.L. Male, M.L. Sanjuan, A. Orera, P.R. Slater, Synthesis and structures of sodium containing $K_{2-x}Na_xMg_2(SO_4)_3$ langbeinite phases, J. Solid State Chem. (2019). doi:10.1016/j.jssc.2019.04.036.

[17] I.A. Trussov, L.L. Male, M.L. Sanjuan, A. Orera, P.R. Slater, Understanding the complex structural features and phase changes in $Na_2Mg_2(SO_4)_3$: A combined single crystal and variable temperature powder di ff raction and Raman spectroscopy study, J. Solid State

Chem. 272 (2019) 157–165. doi:10.1016/j.jssc.2019.02.014.

[18] L. Lander, G. Rousse, D. Batuk, C. V. Colin, D.A. Dalla Corte, J.M. Tarascon, Synthesis, Structure, and Electrochemical Properties of K-Based Sulfates $K_2M_2(SO_4)_3$ with M = Fe and Cu, Inorg. Chem. 56 (2017) 2013–2021. doi:10.1021/acs.inorgchem.6b02526.

[19] P. Barpanda, M. Ati, B.C. Melot, G. Rousse, J.-N. Chotard, M.-L. Doublet, M.T. Sougrati, S.A. Corr, J.-C. Jumas, J.-M. Tarascon, A 3.90 V iron-based fluorosulphate material for lithium-ion batteries crystallizing in the triplite structure, Nat. Mater. 10 (2011) 772–779. doi:10.1038/nmat3093.

[20] G. Oyama, S. Nishimura, Y. Suzuki, M. Okubo, A. Yamada, Off-Stoichiometry in Alluaudite-Type Sodium Iron Sulfate $Na_{2+2x}Fe_{2-x}(SO_4)_3$ as an Advanced Sodium Battery Cathode Material, ChemElectroChem. 2 (2015) 1019–1023. doi:10.1002/celc.201500036.

[21] A.C. Larson, R.B. Von Dreele, General Structure Analysis System (GSAS), Structure. 748 (2004) 86–748. doi:10.1103/PhysRevLett.101.107006.

[22] B.H. Toby, EXPGUI, a graphical user interface for GSAS, J. Appl. Crystallogr. 34 (2001) 210–213. doi:10.1107/S0021889801002242.

[23] J. Gao, X. Sha, X. Liu, L. Song, P. Zhao, Preparation, structure and properties of $Na_2Mn_3(SO_4)_4$: a new potential candidate with high voltage for Na-ion batteries, J. Mater. Chem. A. (2016). doi:10.1039/C6TA02629J.

Figure caption list

Figure 1. Structure of $K_2Mn_2(SO_4)_3$.

Figure 2. PXRD data for $K_{2-x}Na_xMn_2(SO_4)_3$ series (where x = 0-1.4) (Cu $K\alpha_1/K\alpha_2$) showing the successful incorporation of Na

Figure 3. Changes in Mn-O bond length on sodium doping and an image of the langbeinite cage showing the oxygen positions relative to the K1 site

Figure 4. PXRD data for $K_{2-x}Na_xFe_2(SO_4)_3$ (where x = 0 - 1.0) and the difference plot produced from the refinement of $KNaFe_2(SO_4)_3$ (Co $K\alpha_1/K\alpha_2$). Peaks attributed to small unknown impurity phase labelled with '▪'.

Figure 5. X-ray diffraction data for $K_{2-x}Na_xM_2(SO_4)_3$ where M = Co and Ni and x = 0-1.0. (Co Kα1/Kα2), showing incorporation of low levels of Na for M=Co, while the M=Ni system shows high levels of $Na_2Ni(SO_4)_2$ suggesting limited Na incorporation.

Figure 6a. Variation in cell parameter data with Na content (x) for $K_{2-x}Na_xM_2(SO_4)_3$ (Impure samples are denoted with triangles in the plot below) and **6b**. A plot of electronegativity of the divalent metal site vs maximum sodium incorporation (Note: For Ni, the Na incorporation has been assumed to be 0, although cell parameters suggest a very low level of incorporation (it is difficult to determine the exact sodium concentration due to the large number of impurity phases observed in these Ni systems))

Figure 7. PXRD for mixed Mn/Mg langbeinite compositions ($K_{0.5}Na_{1.5}Mn_{1.5}Mg_{0.5}(SO_4)_3$ and $K_{0.25}Na_{1.75}Mn_{2-x}Mg_x(SO_4)_3$ where x = 0.25-1.0) (Cu $K\alpha_1/K\alpha_2$).

Figure 8. PXRD data for $K_{0.5}Na_{1.5}Fe_{1.5}Mg_{0.5}(SO_4)_3$ and $K_{0.5}Na_{1.5}Mn_{1.5}Mg_{0.5}(SO_4)_3$. (Cu $K\alpha_1/K\alpha_2$).

Figure 9. New plot of electronegativity of the divalent metal vs maximum sodium incorporation including compositions that have successfully undergone Mg doping.

Table 1. Cell parameters for $K_{2-x}Na_xMn_2(SO_4)_3$ where x = 0-1.3

Composition	a (Å)	Cell volume (Å^3)
$K_2Mn_2(SO_4)_3$	10.10728(9)	1032.53(3)
$K_{1.5}Na_{0.5}Mn_2(SO_4)_3$	10.0359(3)	1010.81(9)
$K_{1.0}Na_{1.0}Mn_2(SO_4)_3$	9.9705(5)	991.2(2)
$K_{0.9}Na_{1.1}Mn_2(SO_4)_3$	9.9628(2)	988.88(7)
$K_{0.8}Na_{1.2}Mn_2(SO_4)_3$	9.9510(3)	985.36(8)
$K_{0.7}Na_{1.3}Mn_2(SO_4)_3$	9.9392(3)	981.87(8)

Table 2. Cell parameters for $K_{2-x}Na_xFe_2(SO_4)_3$ (where x = 0 - 1.0)

Composition	a (Å)	Cell volume (Å^3)	Impurities (wt%)
$K_2Fe_2(SO_4)_3$	10.0127(3)	1003.8(1)	$FeSO_4$ (7), K_2SO_4 (6)
$K_{1.5}Na_{0.5}Fe_2(SO_4)_3$	9.9992(4)	999.8(1)	Fe_3O_4 (9)
$K_{1.0}Na_{1.0}Fe_2(SO_4)_3$	9.9311(4)	979.5(1)	Unknown

Table 3. Cell parameters for $K_{2-x}Na_x(Co/Ni)_2(SO_4)_3$ (where x = 0 - 1.0)

Composition	a (Å)	Cell volume (Å^3)	Impurities (wt%)
$K_2Co_2(SO_4)_3$	9.9323(4)	979.83(5)	-
$K_{1.5}Na_{0.5}Co_2(SO_4)_3$	9.8802(1)	964.48(4)	-
$KNaCo_2(SO_4)_3$	9.8725(5)	962.2(1)	$Na_2Co(SO_4)_2$ (20) /$CoSO_4$ (8)
$K_2Ni_2(SO_4)_3$	9.8431(5)	953.7(2)	$NiSO_4$ (4), K_2SO_4 (4)
$KNaNi_2(SO_4)_3$	9.807(1)	943.1(4)	$NiSO_4$ (32), K_2SO_4 (2), $Na_2Ni(SO_4)_2$ (10)

Table 4. Cell parameters for manganese systems doped with magnesium

Composition	a (Å)	Cell volume (Å^3)
$K_{0.25}Na_{1.75}Mn_{1.75}Mg_{0.25}(SO_4)_3$	9.8710(5)	961.8(1)
$K_{0.25}Na_{1.75}Mn_{1.5}Mg_{0.5}(SO_4)_3$	9.8382(6)	952.2(2)
$K_{0.25}Na_{1.75}Mn_{1.25}Mg_{0.75}(SO_4)_3$	9.8147(2)	945.43(5)
$K_{0.25}Na_{1.75}MnMg(SO_4)_3$	9.7966(3)	940.20(8)
$K_{0.5}Na_{1.5}Mn_{1.5}Mg_{0.5}(SO_4)_3$	9.8692(1)	961.29(4)

Figure 1. Structure of $K_2Mn_2(SO_4)_3$

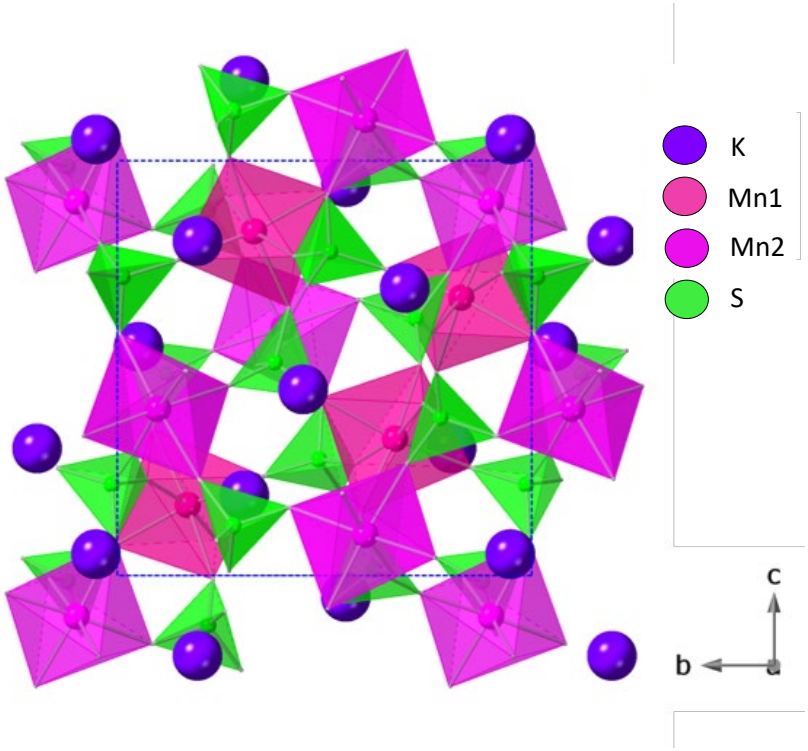

Figure 2. PXRD data for $K_{2-x}Na_xMn_2(SO_4)_3$ series (where x = 0-1.4) (Cu $K\alpha_1/K\alpha_2$) showing the successful incorporation of Na

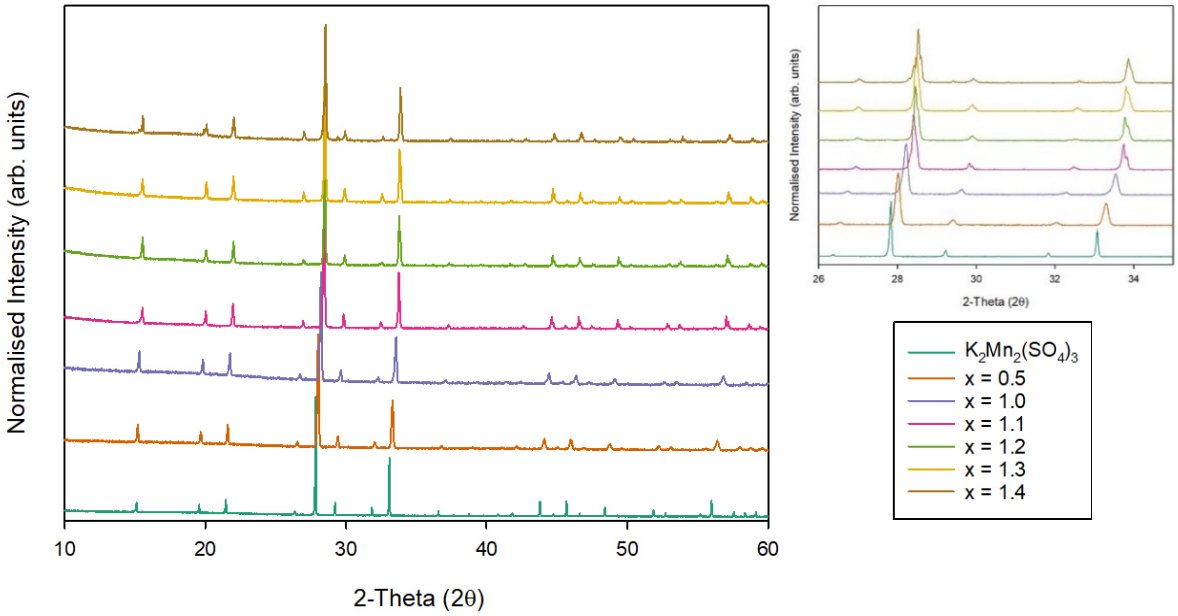

Figure 3. Changes in Mn-O bond length on sodium doping and an image of the langbeinite cage showing where the oxygen positions are relative to the K1 site.

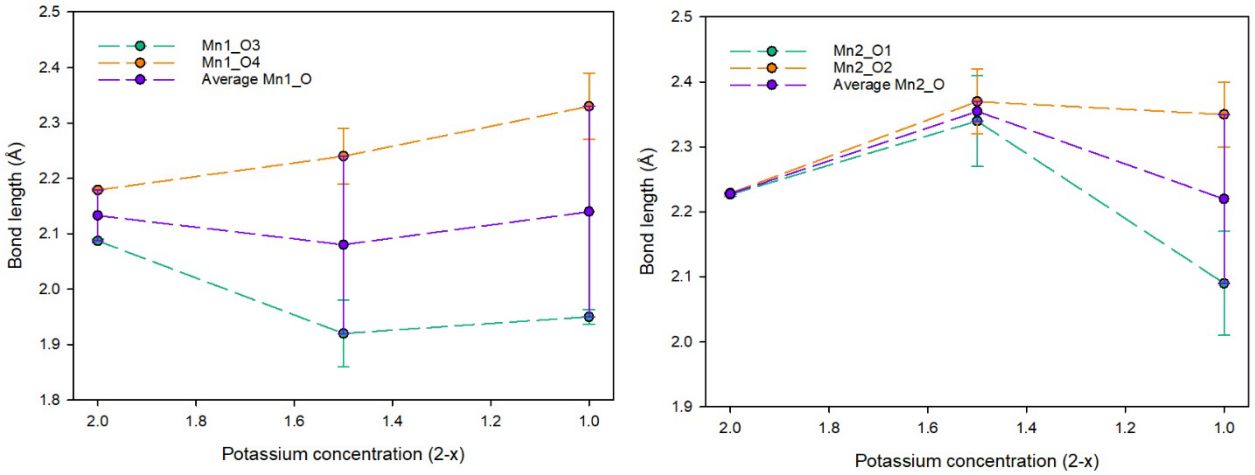

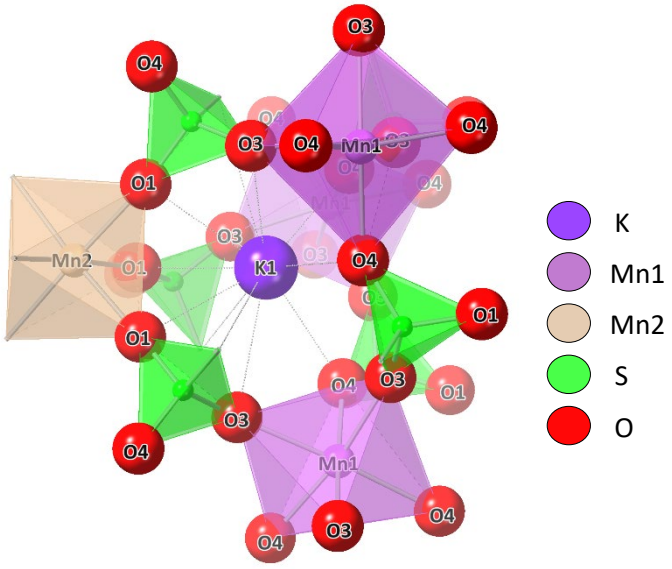

Figure 4. PXRD data for $K_{2-x}Na_xFe_2(SO_4)_3$ (where x = 0 - 1.0) and the difference plot produced from the refinement of $KNaFe_2(SO_4)_3$ (Co $K\alpha_1/K\alpha_2$). Peaks attributed to small unknown impurity phase labelled with '▪'.

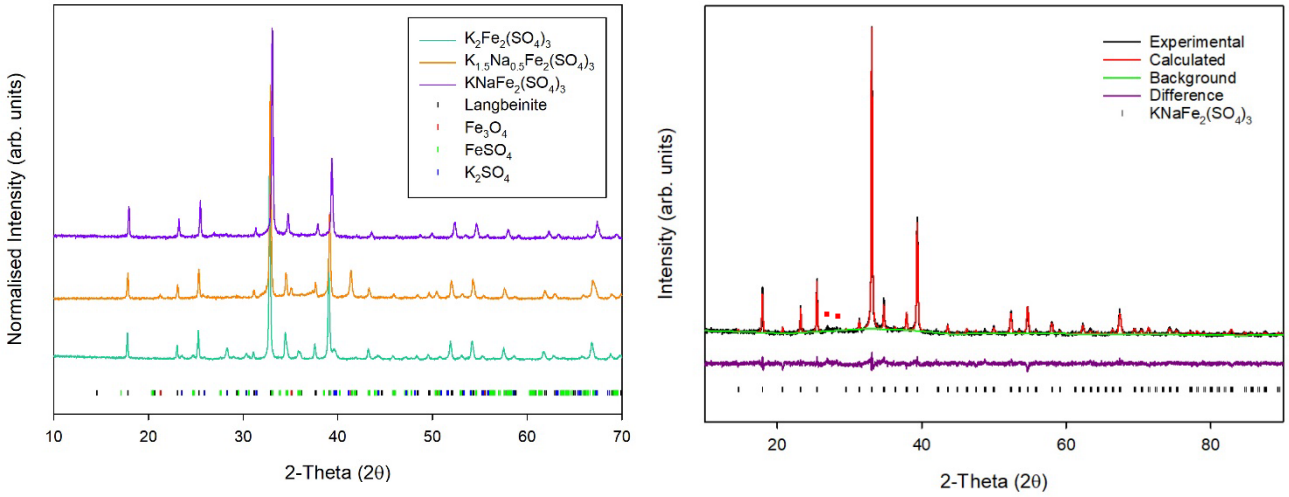

Figure 5. X-ray diffraction data for $K_{2-x}Na_xM_2(SO_4)_3$ where M = Co and Ni and x = 0-1.0. (Co $K\alpha_1/K\alpha_2$), showing incorporation of low levels of Na for M=Co, while the M=Ni system shows high levels of $Na_2Ni(SO_4)_2$ suggesting limited Na incorporation.

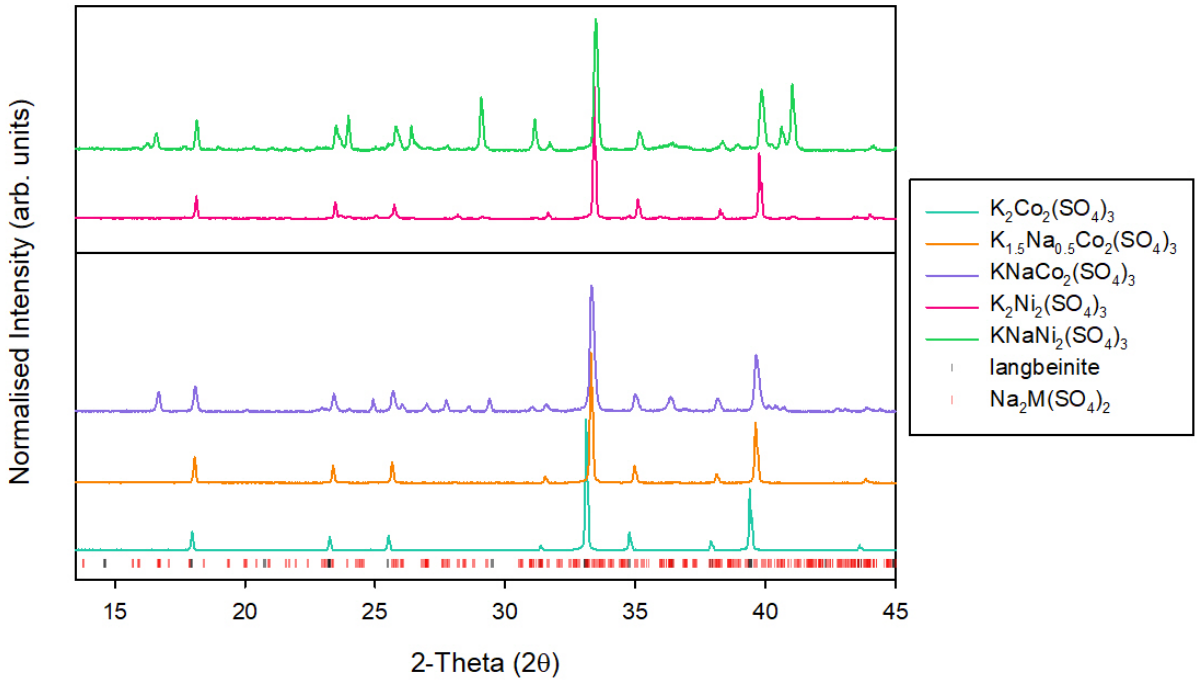

Figure 6a. Variation in cell parameter data with Na content (x) for $K_{2-x}Na_xM_2(SO_4)_3$ (Impure samples are denoted with triangles and Mg values are shown as squares to distinguish these values from the transition metals series in the plot below) and **6b**. A plot of electronegativity of the divalent metal vs maximum sodium incorporation (Note: For Ni, the Na incorporation has been assumed to be 0, although cell parameters suggest a very low level of incorporation (it is difficult to determine the exact sodium concentration due to the large number of impurity phases observed in these Ni systems))

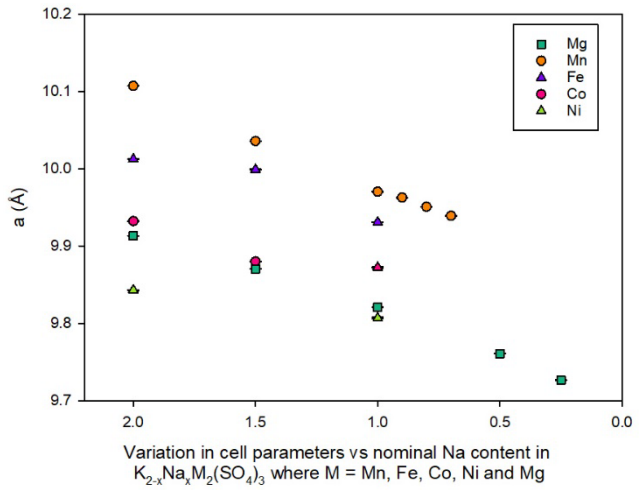

(a)

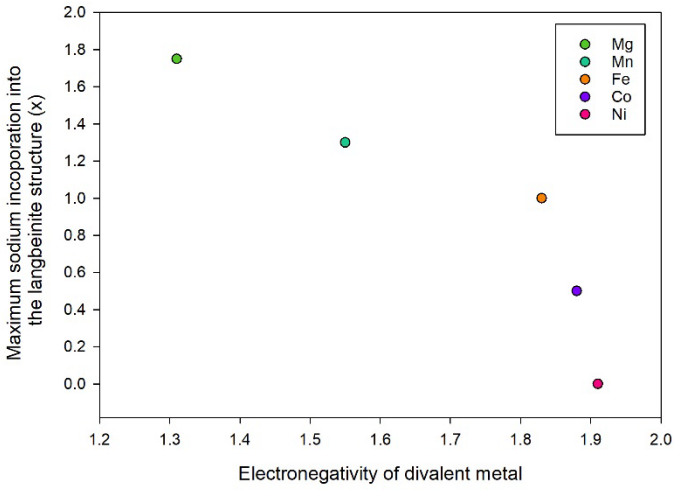

(b)

Figure 7. PXRD for mixed Mn/Mg langbeinite compositions $K_{0.5}Na_{1.5}Mn_{1.5}Mg_{0.5}(SO_4)_3$ (single phase langbeinite) and $K_{0.25}Na_{1.75}Mn_{2-y}Mg_y(SO_4)_3$ where y = 0.25-1.0) (Cu $K\alpha_1/K\alpha_2$), showing a reduction of impurity levels with increasing Mg content until a single phase langbeinite is obtained for y=1.

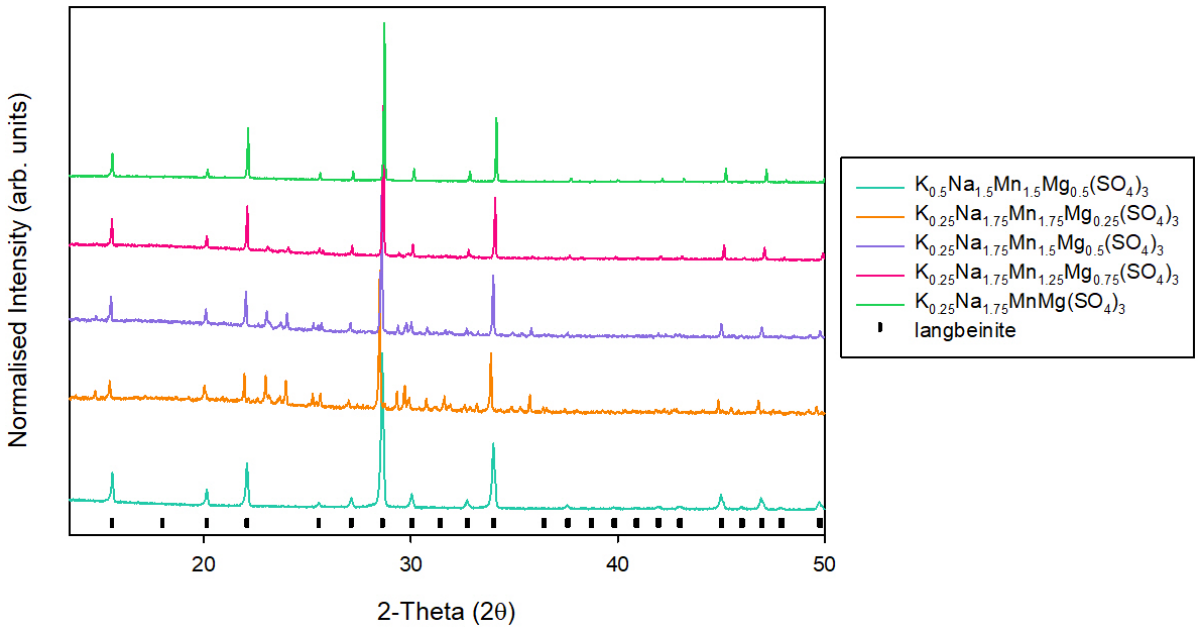

Figure 8. PXRD data for $K_{0.5}Na_{1.5}Fe_{1.5}Mg_{0.5}(SO_4)_3$ and $K_{0.5}Na_{1.5}Mn_{1.5}Mg_{0.5}(SO_4)_3$. (Cu $K\alpha_1/K\alpha_2$).

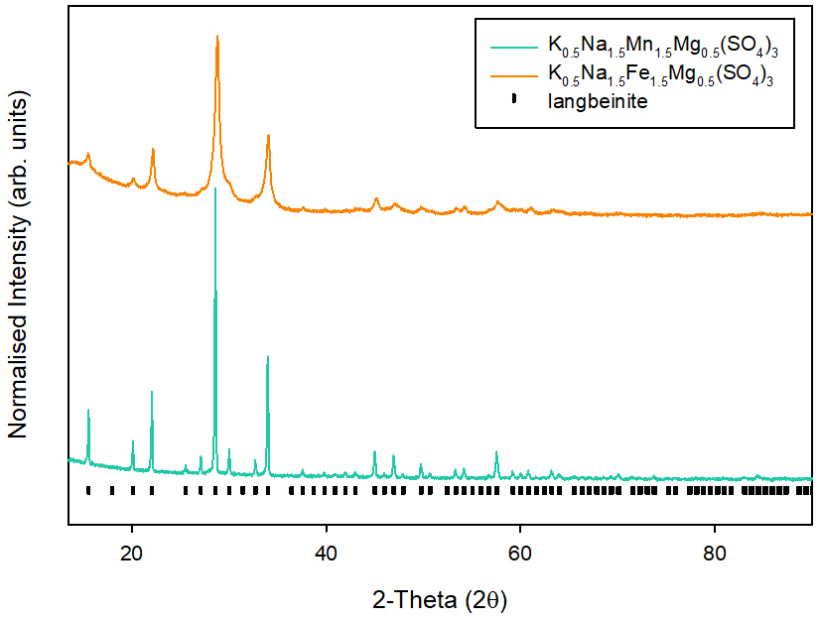

Figure 9. Revised plot of average electronegativity of the divalent metal vs maximum sodium incorporation including compositions that have successfully undergone co-doping with Mg.